Parametric vs. Nonparametric Identification of Nonlinear Acoustic Scattering at Duct Discontinuities based on LES data

By C. Sovardi†, S. Jaensch†, K. Förner†, F. Selimefendigil‡ AND W. Polifke¶

Lehrstuhl für Thermodynamik, Technische Universität München
Boltzmannstr. 15, 85748 Garching b. München

The present study focuses on the analysis of the nonlinear acoustic scattering at an orifice in a duct using numerical simulation and system identification methods. At first, Large Eddy Simulation of a turbulent compressible flow with superimposed acoustic perturbations is performed. Subsequently the acoustic perturbation time series, extracted from the previous simulation, are post-processed with system identification techniques in order to identify the acoustic scattering matrix and to construct linear/nonlinear dynamic models of the system analyzed. A linear dynamic model is obtained with the classic correlation analysis and has been used as reference to point out the effect of nonlinearities on the acoustic scattering. Nonlinear dynamic models are obtained by merging acoustic input-output data sets for either a range of amplitudes when the forcing frequency is fixed or for a range of frequency when the superimposed fluctuating amplitude is fixed. A first estimation of the coefficients of the acoustic scattering matrix in the nonlinear regime is reported.

1. Introduction

Thermoacoustic instabilities in rocket engines can cause mechanical damages and decrease the performance of the combustion chamber. The complicated interaction between heat release and chamber acoustics determines the stability limits of self excited oscillations, the response to finite amplitude perturbations, as well as final amplitude of the pressure oscillation. To increase the losses of oscillation energy and thus obtain more stable operations, acoustic resonators are often attached to the chambers. The dissipation of the acoustic energy is achieved through conversion of acoustic to vortical energy at the resonator mouths and viscous losses along the cavity walls. Generally for the estimation of the acoustic losses, correlations based on the measurements are used. Further progress in passive control of thermoacoustic oscillations requires improved understanding of the physical mechanisms of acoustic damping and accurate methods to characterize quantitatively its nonlinear aspects [1–3].

The present study has been carried out within the context of the summer program SFB/TRR 40 with the financial support of the German Research Foundation (Deutsche

† Ph.D. candidate at Lehrstuhl für Thermodynamik, Technische Universität München
‡ Assis. Prof at Department of Mechanical Engineering, Celal Bayar University, Muradiye
¶ Prof at Lehrstuhl für Thermodynamik, Technische Universität München

Forschungsgemeinschaft – DFG). The work aims to investigate nonlinearities of the acoustic energy dissipation at a duct discontinuity, represented by an orifice. This configuration is simpler than Helmholtz resonators, as typically found in rocket engines, but the flow physics and acoustics share important similarities.

The acoustics of the orifice configuration will be characterized through the acoustic scattering matrix of the system. The scattering matrix is a passive element that contains reflection, transmission and dissipation coefficients of a given acoustic perturbation and can be obtained analytically, numerically or experimentally. Analytical methods are restricted to very simple configurations and most of them do not take into account possible coupling between turbulence and acoustic fluctuations. To consider this coupling, experimental analysis are generally considered; nevertheless typical experimental set-ups are too expensive, especially for preliminary analysis. Numerical investigations, on the contrary, are suitable to study systems with the aforementioned interaction with affordable costs. All these numerical methods are based on the numerical solution of the Navier-Stokes Equations of different levels of approximation. Methods based on Linearized-Euler equations LEEs [4], or Linearized-Navier-Stokes equations LNSEs, [5–7] allow us to compute the acoustic scattering matrix that takes into account the interaction between the mean turbulent flow field and the noise propagation. However these methods are based on a linearization around a mean flow and do not consider the effect of hydrodynamic modes, which may modify the mean flow field, the scattering of sound into turbulence (also called backscattering) and possible nonlinearities.

To address these problems, Polifke and co-workers have developed the method of CFD/SI [8–12] where time series data from a CFD simulation excited by a broadband acoustic signal are post-processed with system identification (SI) techniques to determine the acoustic scattering matrix of the system.

The latter developments on this approach consider a CFD simulation based on Large Eddy Simulation (LES) of compressible flow, allows a reliable numerical computation of turbulent flow field and their interaction with acoustic pressure fluctuations. The LES/SI procedure has been applied to analyse the scattering behaviour of different pipe system configurations, e.g. sudden area expansion [13], T-junctions [14] and cylindrical orifice [15]. Such configurations were characterized by an important interaction between shear layers and the surrounding acoustic field. Enhancement or damping mechanisms of acoustic waves was studied. The same methodology has been applied to the analysis of thermo-acoustic instabilities and to the identification of the flame transfer function (FTF) [16–20]. A correct computation of the turbulent flow field and its interaction with acoustic pressure fluctuations through LES requires high resolution meshes, that may take into account the smallest turbulent structure of the flow field.

In this study a dynamic model characterizing the acoustic scattering at an orifice is obtained combining LES with system identification techniques. The use of nonlinear identification methods is explored to obtain a nonlinear dynamic model, which can be used in further analysis of thermoacoustic instabilities (e.g. in the form of a nonlinear boundary impedance). Parametric and nonparametric system identification methodologies are explored [21]. Nonparametric system identification techniques let to identify dynamic models of the system without defining an a priori model structure and are useful for preliminary analysis on the system dynamic. Parametric models on the other hand require the definition of a given model structure, but the parameter to identify are less w.r.t. the nonparametric ones. Classical techniques, in linear acoustic, to assess the acoustic scattering of a given configuration consist in imposing an acoustic perturbation

to the system and post-process the data series with System identification techniques. Different approaches may be possible. A classical method consist in perturbing the system with sinusoidal excitations at a given frequency and amplitude according to the two source location method [22] and identify the system dynamic in frequency domain for different discrete frequencies. The approach of Polifke and co-workers is based on the other hand on a single broadband excitation which is afterwards post-processed with nonparametric or parametric time domain system identification methods.

The proposed project aimed to analyse the system considering nonlinear identifications of the scattering of the acoustic at the orifice for both sinusoidal and broadband excitation signals. During the time of the summer school program we had to limit our perspective, because of high computational efforts required. However a first estimation of the nonlinear acoustic scattering has been studied for discrete frequencies and has been compared with the linear conditions. Parametric and nonparametric system identification in nonlinear regime techniques have been applied for different sinusoidal excitation signals. A first estimation of the nonlinear dynamics of the system has been therefore assessed.

In Sec. (2) the geometry and the flow conditions are reported. In Sec. (3) the flow simulation details are summarized. In Sec. (4), a brief review of the basic duct acoustic notions is given. Then the LES-SI method is explained both in case of linear and nonlinear SI considered. In Sec. (6) the results of linear and nonlinear SI are reported and discussed and a first estimation of the transmission and reflection coefficients of the acoustic scattering matrix for different discrete frequencies and amplitudes is reported

2. Geometry and Flow Conditions

The configuration analyzed is a duct with diameter D in which an orifice of diameter d and thickness t has been introduced. The length of the whole pipe L is divided by the orifice in two sections of length L_u upstream and L_d downstream, see Fig. (1).

This configuration has been analyzed considering an air flow mean velocity U_{mean}, with constant outlet pressure p_0 and constant Temperature T_0. The geometrical and the flow parameters are reported in Tab. (2).

3. Flow simulation

The turbulent flow inside the orifice under analysis has been simulated by means of the solver AVBP, developed by CERFACS †. This code lets to perform a Large Eddy Simulation (LES) of the three-dimensional compressible Navier-Stokes equations on unstructured meshes. The large turbulent eddies are resolved, whereas the small scales are modelled with a subgrid-scale model. In the present work the WALE (Wall Attached Layer Eddy) subgrid–scale model developed by Nicoud and Ducros [23] is adopted. The numerical discretization scheme adopted is the Lax-Wendroff method. The computational grid consists of a hexahedral mesh used for both the linear and the nonlinear analysis. The grid has been refined in proximity of the orifice to take into account the most important turbulent structures that have a relevant influence on the acoustic dynamics of the present configuration. In axial direction a maximal grid spacing of 1.94×10^{-3} m has been considered in order to have at least 35 grid points per wavelength for the maximum frequency considered ($5000Hz$ in the linear analysis) In radial

† www.cerfacs.fr/4-26334-The-AVBP-code.php

Symbol	Value
f	$[500 \quad 750 \quad 1000 \quad 1250 \quad 1500 \quad 1750 \quad 2000 \quad 2250 \quad 2500 \quad 2750] Hz$
A	$[40\% \quad 50\% \quad 60\% \quad 70\% \quad 80\%] \quad U_{mean}$

TABLE 1. Sinusoidal excitations Amplitudes and Frequencies.

direction the grid has been refined near the wall in order to have the first node at $y^+ = 50$. Therefore the turbulent boundary layer has been modeled with the use of the logarithmic law of the wall. The smallest grid cell is 3.6×10^{-4} m, and the whole domain contains $1,72$ millions of cells. The time step has been fixed to 3.65×10^{-7} s after some preliminary computations, till the steady flow condition, in order to have a Courant-Friederichs-Lewy number (CFL) of 0.7.

The inlet flow profile has been defined according to the power law:

$$U(r) = U_{CL}\left(1 - \frac{r}{R}\right)^{1/7} \tag{3.1}$$

where U_{CL} is the centerline velocity.

In order to obtain reliable results with the SI methodologies used in this work, acoustic waves must not be reflected at the boundaries of the computational domain. To achieve this goal, a modified version of the Navier-Stokes Characteristic Boundary Conditions (NSCBCs) [24] is adopted. This technique, developed by ([25], [26]) is known as Plane Wave Masking, and is suitable for low frequencies regimes, i.e. for frequencies at which planar waves are still present. It should be noted that by means of the classical NSCBC it is impossible to reach perfect non-reflecting acoustic conditions. Input acoustic fluctuations will be imposed at the boundaries as planar wave perturbations, whose maximum frequency (cut-off frequency) has been established to not excite the first (and higher) transverse modes. In nonlinear acoustic regime it must be noticed that high harmonics w.r.t the fundamental imposed may be present, so the input signal must be limited further such that the higher harmonic does not excite the high order modes inside the configuration. Indeed for a correct SI, it is necessary that only plane waves propagate whereas high order modes should decay along the duct.

Two input signals are applied to the inlet and to the outlet of the computational domain. The excitations are imposed as time derivatives of the ingoing characteristics wave amplitudes. The amplitude of the signals considered for the identification of the scattering matrix in the linear regime is scaled to be 1.45% of the mean flow velocity U_{mean} in order to not generate nonlinear responses of the shear layers at the orifice. For the nonlinear analysis, sinusoidal signal with larger amplitudes are considered. The different amplitudes and frequencies of the sinusoidal signals considered are reported in Tab. (1). It could be noticed that the amplitude adopted for the nonlinear system identification is much higher w.r.t the one adopted for the linear case. Indeed it is necessary to use really high amplitudes in order to trigger nonlinearities in this kind of systems. The length of the broadband signal considered is 0.26 s in order to have enough information from the dataset to correctly identify the system.

The output acoustic waves have been extracted on the computational domain at the boundaries by using a Characteristic Based Filter (CBF) [27]. Therefore 6 monitor planes

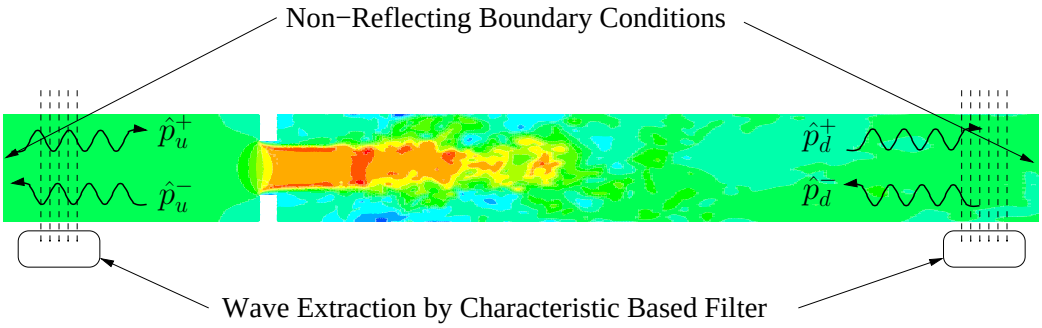

FIGURE 1. Numerical Plane wave extraction scheme.

Symbol	Expression	Value
D	–	$3 \times 10^{-2} m$
d	–	$1.5^{-2} m$
t	–	$5 \times 10^{-3} m$
L	–	$0.515 m$
L_u	–	$0.150 m$
L_d	–	$0.360 m$
U_{mean}	–	$9 m/s$
M	u/c_0	2.6×10^{-2}
Re	uD/ν	$\simeq 18000$
p_0	–	$101325 Pa$
T_0	–	$298 K$

TABLE 2. Geometrical parameters and operating conditions.

have been positioned at the inlet and 10 monitor planes have been positioned at the outlet of the duct. The distance between two successive monitors planes is 0.003 m.

4. Acoustic Scattering Matrix

The acoustic dynamics of plane acoustic waves for a given duct configuration, in linear regime and below the cut-off frequency, can be described by the scattering matrix:

$$\begin{Bmatrix} \hat{p}_d^+ \\ \hat{p}_u^- \end{Bmatrix} = \begin{bmatrix} T^+ & R^- \\ R^+ & T^- \end{bmatrix} \begin{Bmatrix} \hat{p}_u^+ \\ \hat{p}_d^- \end{Bmatrix} \tag{4.1}$$

where $\hat{p}_i$ is the characteristic pressure wave amplitude of a given acoustic travelling wave, T and R are respectively the transmission and the reflection coefficients. The indexes u and d represent respectively the regions immediately upstream and downstream of a generic acoustic element, in our case an orifice, and "+" or "−" indicate the

directions of propagation of the acoustic waves respectively downstream and upstream w.r.t. the fluid flow.

The characteristic pressure wave amplitude can be related with the acoustic velocity fluctuations u' and with the acoustic pressure fluctuations p' by means of:

$$\hat{p}^{+} = \frac{1}{2}\left(p' + \rho c u'\right) \tag{4.2}$$

$$\hat{p}^{-} = \frac{1}{2}\left(p' - \rho c u'\right) \tag{4.3}$$

In the linear regime and below the cut-off frequency. the transmission and the reflection coefficients of Eq. (4.1) depend on the geometry, flow field, speed of sound and frequency of the incoming waves. The linear regime is limited to really small acoustic perturbations, therefore in the present study the amplitude of the acoustic perturbations considered is large enough to generate nonlinear acoustic conditions as will be explained in next section.

5. The LES-SI approach

In this section the numerical procedure is introduced. The LES-SI method is based on two step analysis:

- an acoustically excited compressible flow simulation,
- an acoustic signal-response analysis with system identification techniques.

In within this study the acoustic analysis has been performed both in linear and nonlinear regimes.

5.1. *System Identification*

System identification methods can be utilized to construct dynamic models from the observation of input-output data sets that may be obtained from an experimental test rig or numerical simulation [21, 28]. Identification methods can generally be classified as parametric and non-parametric. In parametric approaches, the system is described with differential/difference equations, and the aim is to find the parameters of this mathematical description. Well known non-parametric representations are the *Impulse Response* (in the time domain) and the *Frequency Response* (in the frequency domain).

The input-output representation of a Linear, Time-Invariant, system in polynomial form is expressed as [21] :

$$A(z)Q(t) = \frac{B(z)}{F(z)}u(t) + \frac{C(z)}{D(z)}v(t), \tag{5.1}$$

where *A, B*, *C, D, F* are polynomials in terms of *z* , *u* and *Q* are the input and output of the system, and *v* is the error term. *z* is a shift operator namely,

$$zQ(t) = Q(t+1). \tag{5.2}$$

Here, $Q(t+1)$ is a shorthand notation for $Q(t+\Delta t)$, for the time step Δt. This operator simply shifts one step ahead value of the input or output to the current time. The past inputs ($u(t-1), ..., u(t-N_u)$) and outputs ($Q(t-1), ..., Q(t-N_Q)$) are called the *regressors*. Depending on the polynomials used, different model structures appear [21]:

– **FIR** (Finite Impulse Response), $A = C = D = F = 1$

This is the simplest model structure to be considered. The past inputs are used as regressors. The structure results in a linear least square problem for minimizing the cost function (e.g. Euclidean norm of the residual between the actual and the estimated output). It requires many regressors and the convergence rate is slow.

– **ARX** (Auto Regressive with eXogenous input), $C = D = F = 1$

This model structure uses the past inputs and past outputs as regressors. This again results in linear least square description where the cost function needs to be minimized.

– **ARMAX** (Auto Regressive Moving Average with eXogenous input): $D = F = 1$

– **OE** (Output Error): $A = C = D = 1$

The output of the system is the system response to a given input corrupted by white noise.

In the identification, a model structure is selected and the number of past inputs and outputs are specified. A criterion to minimize the difference between the actual output and output from identification are specified in order to get the parameters of the model structures. In an equation error/output error type modeling approach, this criterion results in a linear/nonlinear least square fit. In the identification, a model structure is selected and the number of past inputs and outputs are specified. Identification methods have the following procedures in common [21, 28, 29]:

– **An appropriate choice of the input signal:** The system is excited with a proper signal for the excitation of all relevant modes of interest. Generally, broadband forcing, chirp signals or pseudo random binary sequences, which have white noise characteristics, are used to excite the system for a wide range of frequencies.

– **Model structure selection:** In case of parametric nonlinear system identification, equation error or output error model structures are generally adopted.

– **Selection of the number of past inputs and outputs used in the model structure (the system "memory"):** A priori information about the maximum time lag of the system is helpful. Depending on the maximum frequencies of interest and the time lag of the system under consideration, the number of regressors is specified.

– **An algorithm to minimize the cost function:** The difference between responses of the time series data generated from numerical simulation or experiment and identification is minimized. Marquardt-Levenberg algorithm, Gauss-Newton methods or other nonlinear optimization (genetic algorithms, particle swarm optimization) methods are used.

– **Model Validation:** The identified model is tested against signals which have not been used in the estimation. In a broadband forcing, half of the data is used for the fit (minimization of the cost function) while the other half is used for validation.

5.2. *Linear Identification*

Two broadband statistically independent wavelet signals are simultaneously applied at the inlet and the outlet of the configuration [30]. This kind of signals has been chosen because it presents a good decorrelation with itself and therefore allows to get two uncorrelated input signals. Moreover the adoption of a wavelet-type signal allows to get constant power density in the range of frequency of interest. The acoustic responses to the imposed signals are extracted from the computational domain, at different planes positioned upstream and downstream the orifice with constant time step, in term of average pressure and velocity. The acoustic pressure fluctuations p' and velocity fluctuations

u' are then retrieved applying the characteristic based filter as sketched in Fig. (1). This filter allows us to separate the acoustic fluctuations from the turbulent fluctuations using the property that acoustic plane waves propagate with the speed of sound whereas turbulent fluctuations are convected with a velocity of the same order of the mean flow velocity. The characteristic wave amplitudes $\hat{p}^+_{u,d}$ and $\hat{p}^+_{u,d}$ are then computed from the acoustic pressure and velocity fluctuations with Eq. (4.2) and Eq. (4.3). Considering the linear regime, the system can be seen as a Linear Time Invariant (LTI) System and it is possible to characterize the answer of the system with the non-parametric Finite Impulse Response (FIR) model:

$$y_{SI}(t) = \sum_{l=1}^{L} h(l)u(t-l), \tag{5.3}$$

where $h(l)$ represent the coefficients of the finite impulse response and u is the input of the system considered in the analysis. Assuming Eq. (5.3) correlation analysis leads to the so called Wiener-Hopf Filter equation:

$$\mathbf{\Gamma h} = \mathbf{c}, \tag{5.4}$$

where $\mathbf{\Gamma}$ is the autocorrelation matrix of the inputs, $\mathbf{c}$ is the cross-correlation vector of the inputs and of the outputs, $\mathbf{h}$ is the vector containing the coefficients of the finite impulse response.

By inverting Eq. (5.4) it is possible to compute the impulse response vector:

$$\mathbf{h} = \mathbf{\Gamma}^{-1}\mathbf{c}. \tag{5.5}$$

Finally the z-transform of the finite impulse response gives the coefficients of the scattering matrix of the system 4.1.

5.3. *Nonlinear Identification*

Input-output modeling of the nonlinear systems are generally categorized as nonparametric functional series expansion (Volterra, Wiener series expansion) and parametric (differential/difference equation models, neural network models, polynomial models) [31,32]. Volterra series is the extension of the impulse response of the linear system to the nonlinear case [33,34]. These are the Taylor series expansion applied to functionals. In Hammerstein and Wiener identification methods, a linear dynamic block is connected to a static nonlinear input and/or output block structure [32, 35]. Neural network is a black-box identification method which uses expansion functions through the units (layers) to model the nonlinear in-output relation [29, 36, 37].

The nonlinear dynamic fit is generally expressed as,

$$Q(t) = F(Q(t-1), .., Q(t-N_Q), u(t), ..., u(t-N_u)). \tag{5.6}$$

The function F is linear with respect to its arguments (regressors, $Q(t-i)$, $u(t-j)$) for a linear system. In linear identification, it is not so difficult to obtain a dynamic model using one of the existing model structures and appropriate choice of the excitation signal. For a nonlinear system, the form of the function F is not known a priori. This function is approximated using expansion functions and polynomials. Nonlinear extensions of the linear model structures are named as NFIR, NARX and NARMAX, and NOE [38].

Neural network identification methods belong to parametric nonlinear black box identification procedures [29, 39]. They are promising in the identification of any nonlinearity up to a specified degree of accuracy (universal function approximators). Artificial neural nets (ANN) are composed of connecting processing elements called "neurons". ANN structure are composed of different layers; "input", "hidden" and "output layers". The nodes in the hidden layer perform nonlinear input-output transformations by using different activation functions, e.g., sigmoid, tangent hyperbolic, which are shown in Fig. (2). The weights of the ANN can be adjusted to minimize the difference between the actual outputs and outputs of the neural net with a given topology. Details for modeling with ANN can be found in [39]. Data collection as the input-output to the network, choice of the network architecture, number of neurons, number of hidden layers, activation function, learning algorithm, validation of the data set are the main steps in ANN modeling.

Let φ be the set of regressors with memory length of L, u as the input, y as the output

$$\phi = [1\ u(t-1)\ ....u(t-L)], \tag{5.7}$$

and Z^N be the set of the input-output data (training set) up to time N. Then the identification problem will be formulated as the minimization of the error between the CFD model output and the output from neural network as

$$V_N(\theta) = \frac{1}{N}\sum_{t=1}^{N}[y_{\text{CFD}}(t) - y_{\text{NeuralNet}}(t)]^2. \tag{5.8}$$

This function will be minimized by some nonlinear iterative search algorithms and we use Levenberg-Marquardt technique to find the minimum of the function and hence the weights of neural networks which are denoted by θ . The output from the neural network will be written in terms of the weights of the network as

$$y_{\text{NeuralNet}}(t) = \sum_{j=1}^{M} W_j f(\sum_{l=1}^{L} w_{jl}\phi_l + w_{j0}) + W_0, \tag{5.9}$$

where w and $W's$ are the weights of the neural network for the input and output to the hidden layer and f is the tangent hyperbolic activation function. A topology of the network structure from input layer to the output layer is depicted in Fig. (3).

In this study, two different model structures are used; a nonlinear ARX model structure (NARX) and a Hammerstein model structure which are detailed below:

– **Nonlinear ARX model** :

The nonlinear part of the NARX model is defined as [21]

$$g(x) = \sum_{j=1}^{n} \alpha_j \kappa\left(\beta_j(x - \gamma_j)\right), \tag{5.10}$$

where κ is the wavelet/sigmoid functions of the network and x denotes the vector of regressors defined as

$$x = [y(t-1), y(t-2), ..., y(t-n_a), u(t), .., u(t-n_b)]\,. \tag{5.11}$$

A schematic representation of the NARX model is shown in Fig. (4).

– **Hammerstein Wiener model**:

The block diagram representation of the Hammerstein Wiener model is shown in Fig. (5).

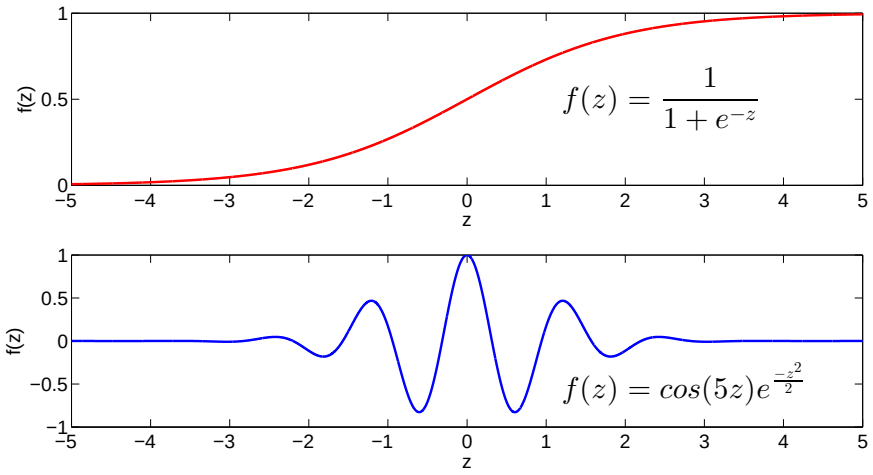

FIGURE 2. Approximation functions used in the nonlinear unit, Sigmoid (above), Wavelet (below) [2].

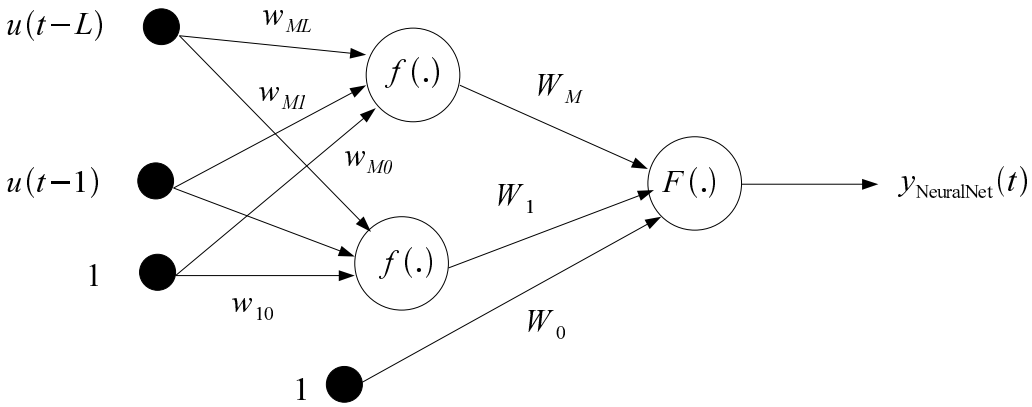

FIGURE 3. 1 hidden layer feed-forward neural network structure along with regressors with tangent hyperbolic activation function f and the linear function F at the output layer, M is the number of units and L is the memory length of the regressors.

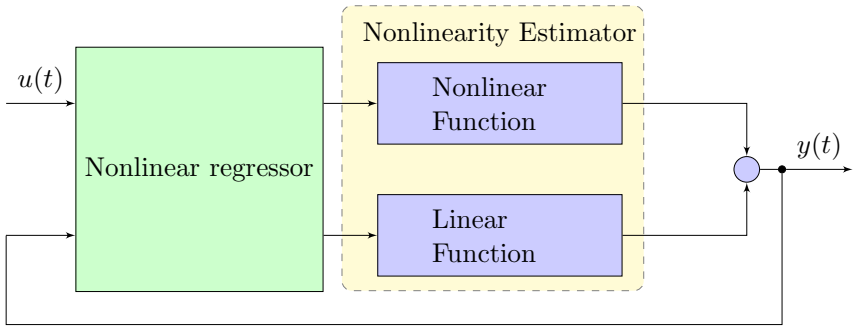

FIGURE 4. NARX model structure [21].

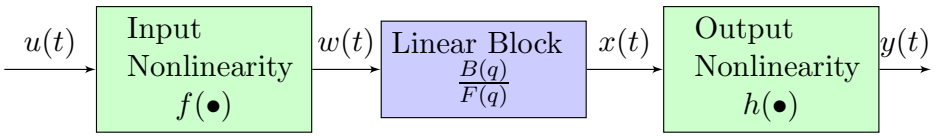

FIGURE 5. Hammerstein Wiener model structure [21].

The input data u is transformed to w by using a nonlinear function f

$$w(t) = f(u(t)). \tag{5.12}$$

The output of the system is obtained by using a linear transfer function and a nonlinear map as

$$x(t) = (B/F)\, w(t), \qquad y(t) = h(x(t)) \tag{5.13}$$

For the nonlinearity estimator wavelet or sigmoid can be used.

6. Results

6.1. *Linear system identification*

In Fig.(6) and in Fig. (6) the absolute value and the phase of the scattering matrix for the linear regime are plotted. Experimental results by [40] and numerical results are compared. The numerical simulations are in a good agreement with the experimental results although it can be observed quite important differences in capturing the peaks at 2000 Hz for the absolute values of the transmission coefficients T^{+} and T^{-}. This is mainly due to the mesh refinement and to the adoption of the logarithmic law of the wall to model the turbulent boundary layer. The grid is not yet enough resolved, and therefore the interaction between turbulence and acoustics is not perfectly captured. Beside the coarseness of the mesh, this kind of set up allows to get the general trend of the acoustic dynamic of the configuration under analysis within moderate time for the simulation. Therefore in order to obtain a preliminary wide-spectra analysis of the acoustic damping at duct discontinuities in nonlinear regimes, has been considered a suitable model.

6.2. *Nonlinear system identification*

In this study, two different configurations are considered for nonlinear identification purpose. In the first configuration, different amplitudes at a constant frequency of 1500 Hz is considered. The parameter estimation has been performed considering three sinusoidal excitation whose amplitudes are 40, 60 and 80 $\%$ of the mean flow velocity. Validation is performed for amplitudes equal to 50 and 70 $\%$ of the mean flow velocity. The estimation/validation data sets with the number of samples and time step size are tabulated in Tab. (3)/Tab. (4).

The time step size is taken as the time step size of the CFD computations. A NARX model structure with 2 inputs and 2 outputs, a MIMO system (u_1, u_2 inputs, y_1, y_2 outputs), is considered. The orders for the regressors as expressed in Eq. (5.6) are $na = [4\ \ 0; 0\ \ 4]$, $nb = [4\ \ 4; 4\ \ 4]$. The nonlinearity estimator for output 1 is a wavenet structure with 4 units and for output 2 is a wavenet structure with 9 units. This model structure is called NL-M1. In order to improve the performance of the nonlinear identification, more nonlinearity is added in terms of the custom regressors. This model structure is called

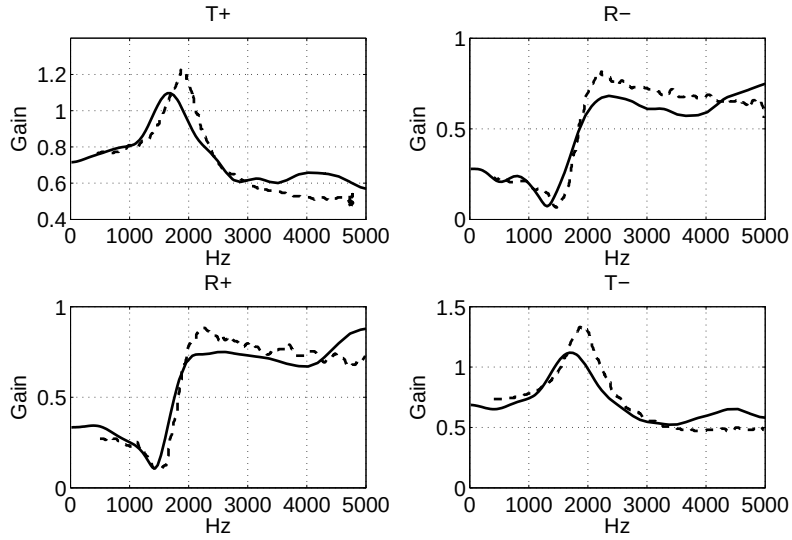

FIGURE 6. Absolute values of the scattering matrix coefficients. Solid lines: Linear system identification results. Dashed lines (–) Experimental results from Testud et al.

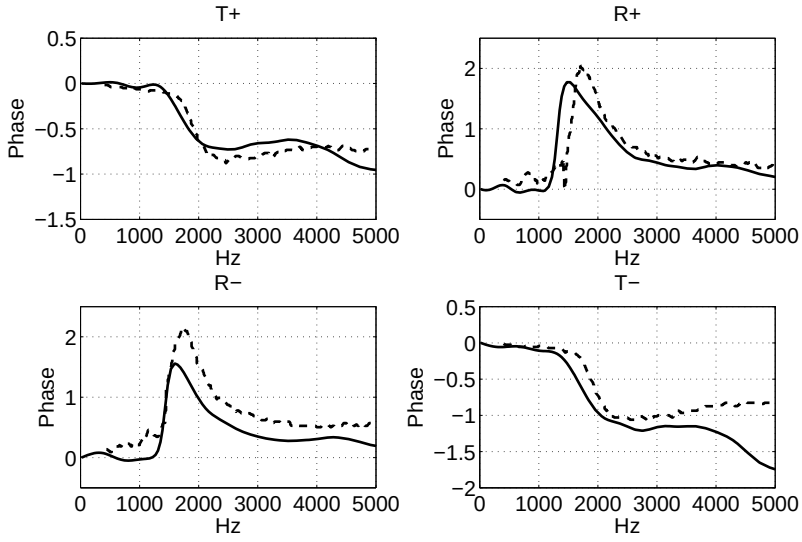

FIGURE 7. Phase of the scattering matrix coefficients. Solid lines: Linear system identification results. Dashed lines (–) Experimental results from Testud et al.

NL-M2. In NL-M2, the added custom regressors for first output y_1 is

$$\begin{aligned}\big[&y_1(t-1)^2, y_1(t-2)^2,\ y_1(t-3)^2, y_1(t-4)^2, \ldots \\ &u_1(t)^2, u_1(t-1)^2, u_1(t-2)^2, u_1(t-3)^2, \ldots \\ &u_2(t)^2, u_2(t-1)^2, u_2(t-2)^2, u_2(t-3)^2\big],\end{aligned}$$

Experiments	Samples	Sampling interval
A=40%	1301	8.75×10^{-6}
A=60%	1301	8.75×10^{-6}
A=80%	1301	8.75×10^{-6}

TABLE 3. Estimation data set for different amplitudes at f=1500 Hz.

Experiments	Samples	Sampling interval
A=50%	1301	8.75×10^{-6}
A=70%	1301	8.75×10^{-6}

TABLE 4. Validation data set for different amplitudes at f=1500 Hz.

Experiments	Samples	Sampling interval
f=500 Hz	751	3.5×10^{-5}
f=1000 Hz	426	3.5×10^{-5}
f=1500 Hz	276	3.5×10^{-5}
f=2000 Hz	176	3.5×10^{-5}
f=2500 Hz	151	3.5×10^{-5}

TABLE 5. Data set used in identification for different frequencies at amplitude of 80%.

and for the second output y_2 is

$$\begin{aligned}\big[&y_2(t-1)^2, y_2(t-2)^2,\ y_2(t-3)^2, y_2(t-4)^2, ... \\ &u_1(t)^2, u_1(t-1)^2, u_1(t-2)^2, u_1(t-3)^2, ... \\ &u_2(t)^2, u_2(t-1)^2, u_2(t-2)^2, u_2(t-3)^2\big]\end{aligned}$$

The nonlinearity estimator for NL-M2 is also a wavenet structure with 8 units for output 1 and 6 units for output 2. The estimated and validated results are shown in Figs. (8) and Fig. (9). In order to compare the performance of the nonlinear identification, the result of linear identification with the same order is also included in the figures. On top of the figures, the fits to the CFD model (reference model) are also added. The best performance both for estimation and validation are obtained with model NL-M2 (nonlinear model with more nonlinearity added through custom regressors).

In the second configuration, cases corresponding to different frequencies at velocity amplitude of 80% of the mean velocity are identified by merging different simulations with a Hammerstein Wiener model structure. The number of samples and time step size of the sampling interval are shown in Tab. (5). The orders of the linear transfer function $n_b = [50\ \ 50; 50\ \ 50]$, $n_f = [0\ \ 0; 0\ \ 0]$. The input nonlinearity estimator is a wavenet structure with 12 units for input1 and 16 units with input 2. Time step size of the identification is taken as four times of the time step size of the CFD computations. The fits between the CFD and predicted outputs are shown in Fig. (10) for frequency of 500 Hz, and for frequency of 2500 Hz. The residuals as shown in Fig. (11) are low and uncorrelated.

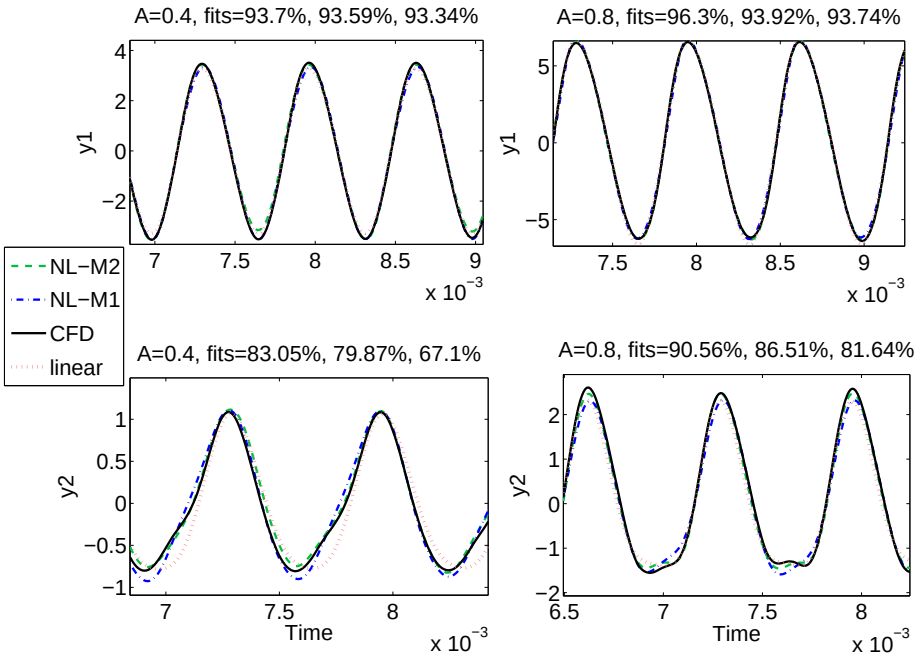

FIGURE 8. Estimation results of linear/nonlinear system identification compared to CFD for different amplitudes at a fixed frequency of 1500 Hz, y1: first output, y2: second output.

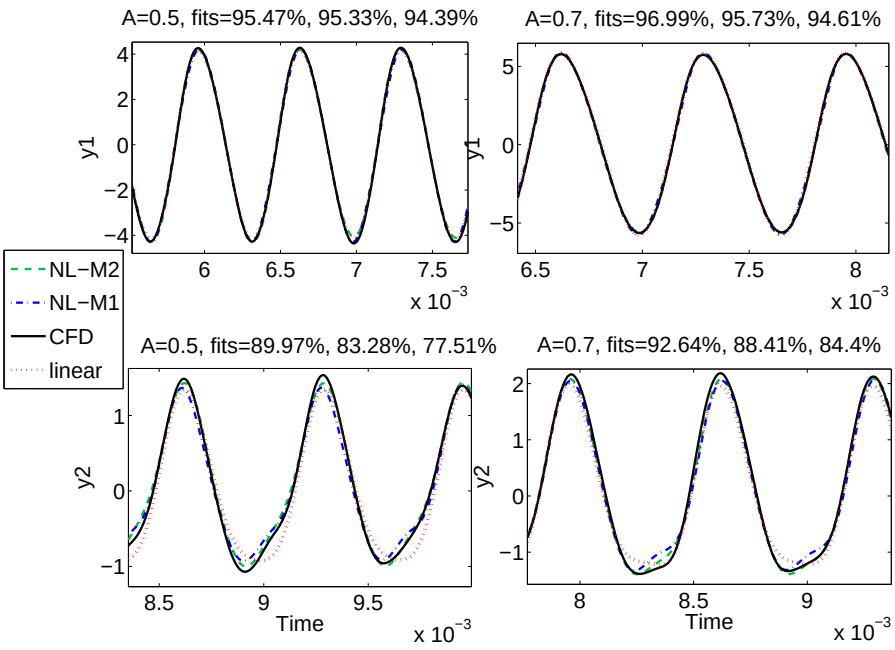

FIGURE 9. Validation results of linear/nonlinear system identification compared to CFD for different amplitudes at a fixed frequency of 1500 Hz, y1: first output, y2: second output.

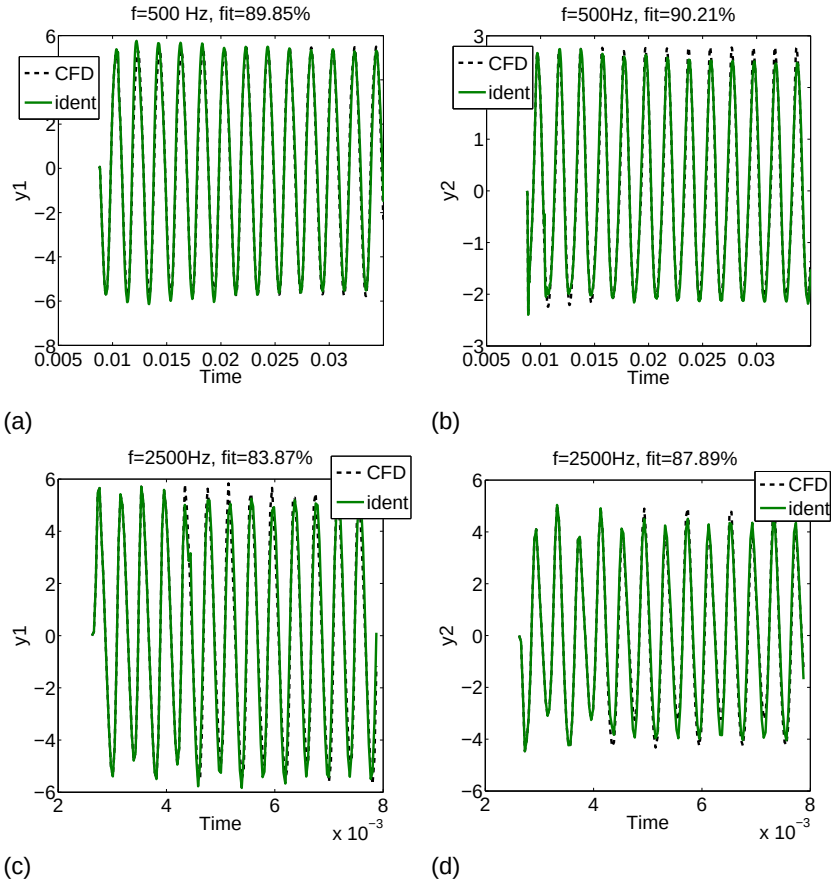

FIGURE 10. Fit between the Hammerstein Wiener system identification and CFD for frequency of 500 Hz (a,b) and 2500 Hz (c,d); y1: first output, y2: second output.

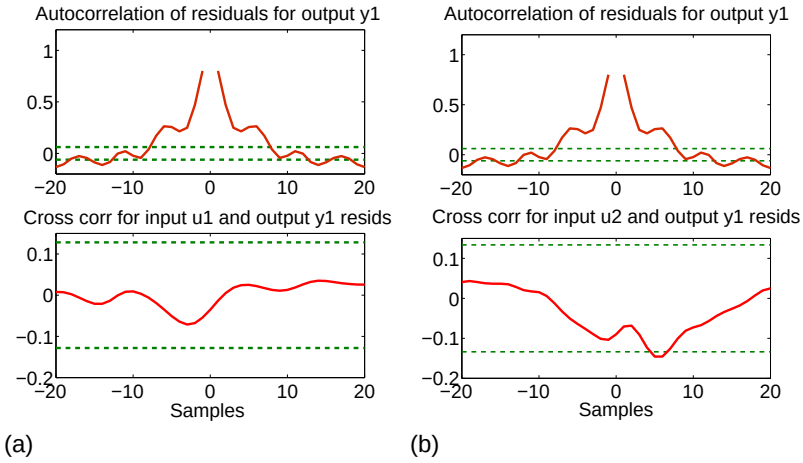

FIGURE 11. Residual autocorrelation and cross-correlation.

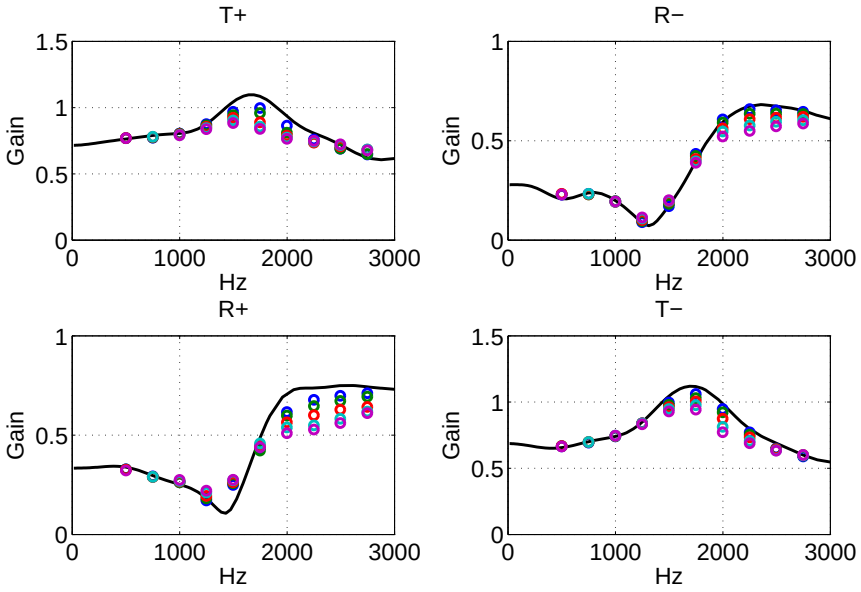

FIGURE 12. Absolute value of the scattering matrix coefficients. Solid lines: Linear system identification results. Non-linear system identification for sinusoidal excitation: blue $0.4U_{mean}$, green $0.5U_{mean}$, red $0.6U_{mean}$, azure $0.7U_{mean}$, purple $0.8U_{mean}$.

6.3. *Acoustic scattering matrix in nonlinear regime*

A first estimation of the acoustic scattering matrix in nonlinear regimes is here reported. The coefficients of the scattering matrix have been computed at the different frequencies and amplitudes as listed in Tab. (1). The methodology adopted in this analysis is based on the "two sources" strategy [22]. In order to get two independent acoustic fields two simulations are required: one with a sinusoidal forcing positioned at the inlet and another with the sinusoidal forcing positioned at the outlet. The coefficients of the scattering matrix are then retrieved in frequency domain, after a Fourier transform of the data series, considering the ratio between the fundamental harmonic of the outputs and the imposed harmonic of the inputs, which have the same frequency, as follows:

$$\begin{bmatrix} T^{+}(\omega) = \dfrac{\hat{p}_d^{+}(\omega)}{\hat{p}_u^{+}(\omega)} & R^{-}(\omega) = \dfrac{\hat{p}_d^{+}(\omega)}{\hat{p}_d^{-}(\omega)} \\ R^{+}(\omega) = \dfrac{\hat{p}_u^{-}(\omega)}{\hat{p}_u^{+}(\omega)} & T^{-}(\omega) = \dfrac{\hat{p}_u^{-}(\omega)}{\hat{p}_d^{-}(\omega)} \end{bmatrix}. \tag{6.1}$$

The gain of the scattering matrix coefficients for the sinusoidal excitation at different amplitudes and frequencies are shown in Fig.(12) whereas the phase of the scattering matrix are shown in Fig. (13).

The nonlinear trend is clearly visible: both gain and phase decrease with increasing amplitude of excitation. The frequency range of whistling potentiality, found by Testud [40] to be around $St = 0.25$ $(1800Hz)$ is characterized by a maximum value of the gain of T^{+} and T^{-} that decreases increasing the amplitude. Therefore the mechanism of sound amplification due to the acoustic-flow field interaction that takes place in the boundary layer [41] is damped in nonlinear regimes.

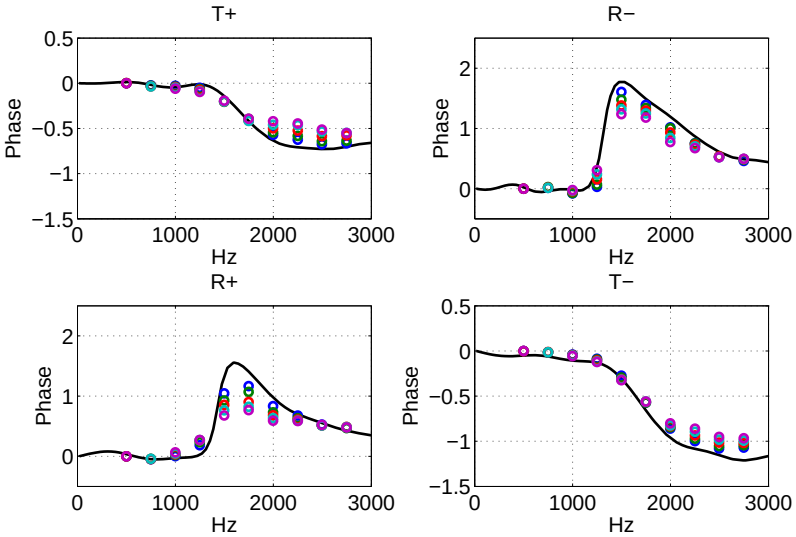

FIGURE 13. Phase value of the scattering matrix coefficients. Solid lines: Linear system identification results. Non-linear system identification for sinusoidal excitation: blue $0.4U_{mean}$, green $0.5U_{mean}$, red $0.6U_{mean}$, azure $0.7U_{mean}$, purple $0.8U_{mean}$.

A first modeling for the acoustic scattering in nonlinear regime has been also considered. The dynamic of the system has been simulated considering the Wiener-Hammerstein model structure Eq. 5.4. The finite impulse response model, identified for the linear system identification, has been adopted as for the linear block in Fig. (5). Nonlinearities in the system have been modeled statically considering two saturation functions for the inputs and two saturation functions for the output. The levels of saturation defined are:

- $[-0.55, \quad 0.55]$ on $\hat{p}_u^+$,
- $[-0.55, \quad 0.70]$ on $\hat{p}_d^-$,
- $[-0.70, \quad 0.55]$ on $\hat{p}_d^+$,
- $[-0.70, \quad 0.55]$ on $\hat{p}_u^-$.

The results for the absolute values of the coefficient of the scattering matrix are reported in Fig. (14). The Wiener-Hammerstein model let to capture the damping on the scattering matrix coefficients in nonlinear conditions. The acoustic scattering matrix coefficients descreases increasing the amplitudes of the excitation. However this model structure in not able to model correctly the dynamic of the system. Indeed it damps the acoustic dynamic for all the frequencies considered, also for frequencies ($f < 1000Hz$) in which none nonlinear effect has been noticed for the sinusoidal excitation analysis.

7. Conclusions

In this study, Large Eddy Simulation of a turbulent compressible flow with superimposed acoustic perturbations is performed for an orifice in a circular duct. System identification methods have been used to construct dynamic models of the considered flow configuration. First a correlation based identification method is used in the linear regime by employing two broadband statistically independent wavelet signals at the inlet and at the outlet of the configuration. The scattering matrix is obtained and it is observed that absolute value and phase of the scattering matrix are in good agreement with the re-

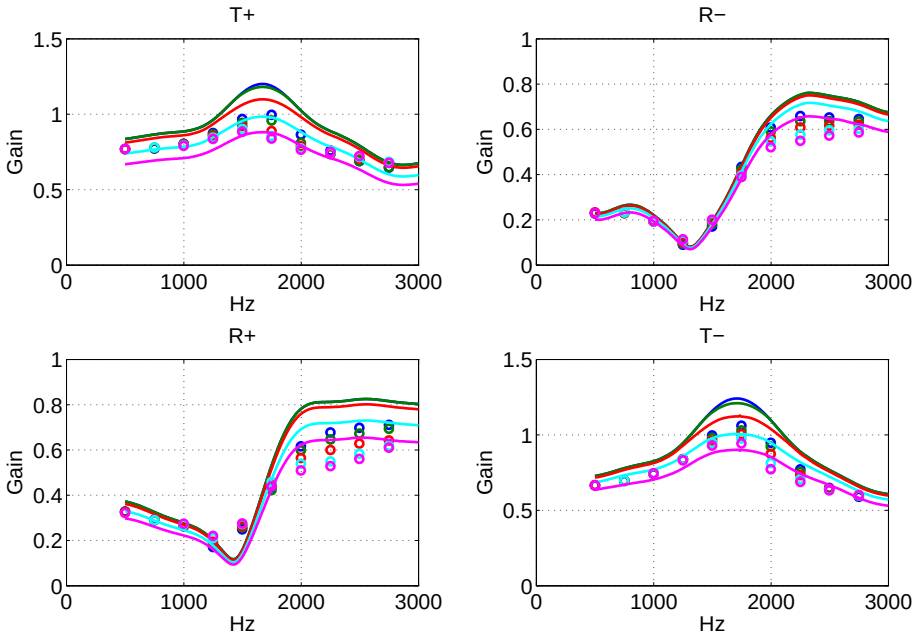

FIGURE 14. Absolute value of the scattering matrix coefficients. Solid lines: Wiener-Hammerstein modelization. Dots: non-linear system identification for sinusoidal excitation. Colors: blue $0.4U_{mean}$, green $0.5U_{mean}$, red $0.6U_{mean}$, azure $0.7U_{mean}$, purple $0.8U_{mean}$.

ported experimental results. Nonlinear dynamical models are constructed merging the data sets obtained a) different amplitudes for a fixed frequency and b) different frequencies at a fixed amplitude. A nonlinear ARX model and a Hammerstein Wiener model structure are employed. The validation tests for these models show that the fits between the CFD model and identified model are good and residuals are low and uncorrelated. These models obtained from the linear/nonlinear identification can be used in further analysis of thermo/ aero-acoustic instabilities. A first estimation of the influence of nonlinearities on the acoustic scattering matrix has been reported and analysed.

Acknowledgments

This project is a part of the Summer School Program SFB-TRR40 (2013). Financial support has been provided by the German Research Foundation (Deutsche Forschungsgemeinschaft – DFG) in the framework of the Sonderforschungsbereich Transregio 40. Computational resources have been provided by the Leibniz Rechenzentrum (LRZ) München.

References

[1] SELIMEFENDIGIL, F. (2010). Identification and Analysis of Nonlinear Heat Sources in Thermo-Acoustic Systems. *Ph.D. thesis*. TU München.

[2] SELIMEFENDIGIL, F., FÖLLER, S. AND POLIFKE, W. (2012). Nonlinear identification of the unsteady heat transfer of a cylinder in pulsating crossflow. *Computers and Fluids*, **53**.

[3] NOIRAY, N., DUROX, D., SCHULLER, T. AND CANDEL, S. (2008). A unified framework for nonlinear combustion instability analysis based on the flame describing function. *J. Fluid Mech.*

[4] RAO, P. AND MORRIS, P. (2006). Use of finite elment methods in frequency domain aeroacoustics. *AIAA Journal*, **44**, 1643–1652.

[5] GIKADI, J., SCHULZE, M., SCHWING, J., FÖLLER, S. AND SATTELMAYER, T (2012). Linearized Navier-Stokes and Euler Equations for the Determination of the Acoustic Scattering Behaviour of an Area Expansion. *18th AIAA/CEAS Aeroacoustics Conference (33rd AIAA Aeroacoustics Conference)*.

[6] KIERKEGAARD, A., BOIJ, G. AND EFRAIMSSON, G. (2012). Simulations of the scattering of sound waves at a sudden area expansion. *J. Sound and Vibration*, **331**, 1068–1083.

[7] PANKIEWITZ, C., FISCHER, A., HIRSCH, C. AND SATTELMAYER, T. (2010). Computation of Transfer Matrices for Gas Turbine Combustors Including Acoustic/Flame Interaction.

[8] FÖLLER, S., KAESS, R. AND POLIFKE, W. (2010). Determination of Acoustic Scattering Coefficients via Large Eddy Simulation and System Identification *High Performance Computing in Science and Engineering*.

[9] FÖLLER, S., KAESS, R. AND POLIFKE, W. (2008). Reconstruction of Acoustic Transfer Matrices from Large-Eddy-Simulations of Complex Turbulent Flows. *14th AIAA/CEAS Aeroacoustics Conference (29th AIAA Aeroacoustics Conference)*.

[10] GENTEMANN, A. M. G., FISCHER, A., EVESQUE, S. AND POLIFKE, W. (2003). Acoustic Transfer Matrix Reconstruction and Analysis for Ducts with Sudden Change of Area. *9th AIAA/CEAS Aeroacoustics Conference*.

[11] POLIFKE, W. (2008). *Identification of thermo- and aero-acoustic response functions from CFD time series*.

[12] POLIFKE, W., PONCET, A., PASCHEREIT, C. O. AND DÖBBELING, K. (2001). Reconstruction of Acoustic Transfer Matrices by Instationary Computational Fluid Dynamics. *J. Sound and Vibration*, **245**, 483–510.

[13] FÖLLER, S. AND POLIFKE, W. (2012). Identification of Aero-Acoustic Scattering Matrices from Large Eddy Simulation: Application to a Sudden Area Expansion of a Duct. *J. Sound and Vibration*, **331**, 3096–3113.

[14] FÖLLER, S., POLIFKE, W. AND TONON, D. (2010). Aero-Acoustic Characterization of T-Junctions Based on Large Eddy Simulation and System Identification. *16th AIAA/CEAS Aeroacoustics Conference*.

[15] LACOMBE, R., MOUSSOU, P., FÖLLER, S., JASOR, G., POLIFKE, W. AND AUREGAN, Y. (2010). Experimental and Numerical Investigations on the whistling ability of an orifice in flow duct. *ICSV 17*.

[16] TAY-WO-CHONG, L., BOMBERG, S., ULHAQ, A., KOMAREK, T. AND POLIFKE, W. (2012). Comparative Validation Study on Identification of Premixed Flame Transfer Function. *J. Eng. Gas Turbines Power*, **17**.

[17] TAY-WO-CHONG, L., BOMBERG, S., ULHAQ, A., KOMAREK, T. AND POLIFKE, W. (2011). Comparative Validation Study on Identification of Premixed Flame Transfer Function. *Proceedings of ASME Turbo Expo 2011*.

[18] POLIFKE, W. (2011). Combining LES with system identification for the analysis

of flame dynamics. *2011 LES Combustion Symposium*.

[19] TAY-WO-CHONG, L., KAESS, R., KOMAREK, T., FÖLLER, S. AND POLIFKE, W. (2010). Identification of Flame Transfer Functions Using LES of Turbulent Reacting Flows. *High Performance Computing in Science and Engineering*, 255–266.

[20] TAY-WO-CHONG, L., KAESS, R., KOMAREK, T., FÖLLER, S. AND POLIFKE, W (2009). Identification of Flame Transfer Functions Using LES of Turbulent Reacting Flows. *High Performance Computing in Science and Engineering*.

[21] LJUNG, L. (1987). *System Identification: Theory for the User.* Englewood Cliffs.

[22] ABOM, M. (1992). A note on the experimental determination of the acoustical two-port matrices. *J. Sound and Vibration*.

[23] NICOUD, F. AND DUCROS, F. (1999). Subgrid-scale stress modelling based on the square of the velocity gradient tensor. *Flow, Turbulence and Combustion*.

[24] POINSOT, T. J. AND LELE, S. K. (1992). Boundary Conditions for Direct Simulation of Compressible Viscous Flows. *J. Computational Physics*, **101**, 104–129.

[25] KAESS, R., HUBER,A. AND POLIFKE, W. (2008). A Time-Domain Impedance Boundary Condition for Compressible Turbulent Flow. *14th AIAA/CEAS Aeroacoustics Conference (29th AIAA Aeroacoustics Conference)*.

[26] POLIFKE, W., WALL, C. AND MOIN, P. (2006). Partially Reflecting and Non-Reflecting Boundary Conditions for Simulation of Compressible Viscous Flow. *J. of Comp. Phys*, **213**, 437–449.

[27] KOPITZ, J., BRÖCKER E. AND POLIFKE, W. (2005). Characteristic based filter for identification of planar acoustic waves in numerical simulation of turbulent compressible flow gradient tensor. *12th International Congress of Sound and Vibration*.

[28] SÖDERSTRÖM, T. AND STOICA, P. (1989). *System Identification.* Prentice-Hall International.

[29] SJÖBERG, J., ZHANG, Q., LJUNG, L., BENVENISTE, A., DELYON, GLORENNEC, P. Y., HJALMARSSON, H. AND JUDITSKY, A. (1995). Nonlinear black-box modeling in system identification: a unified overview. *Automatica*, **31**, 1691–1724.

[30] FÖLLER,S. AND POLIFKE, W. (2011). Advances in Identification Techniques for Aero-acoustic scattering coefficients from Large Eddy Simulation. *18th International Congress of Sound and Vibration*.

[31] NOWAK, R. D. (2002). Nonlinear system identification. *Circuits, Systems, and Signal Processing*, **21**, 109–122.

[32] BILLINGS, S. A. (1980). Identification of Nonlinear Systems - A Survey. *Proceedings of IEEE*.

[33] BOYD, S. AND CHUA, L. O. (1985). Fading Memory and the Problem of Approximating Nonlinear Operators with Volterra Series. *IEEE Transactions on Circuits and Systems*, **32**, 1150–1161.

[34] RUGH, W. J. (1981). *Nonlinear System Theory.* The Johns Hopkins University Press.

[35] KORENBERG, M. J. (2009). Parallel cascade identification and kernel estimation for nonlinear systems. *Annals of Biomedical Eng.*, **19**, 429–455.

[36] NARENDRA, K. AND PARTHASARATHY, K. (1990). Identification and Control of Dynamical Systems Using Neural Networks. *IEEE Transactions on Neural Networks*, **1**, 4–27.

[37] NØRGAARD, M., RAVN, O. AND POULSEN, N. K. (2002). NNSYSID-toolbox for System Identification with Neural Networks. Mathematical and Computer Modelling of Dynamical Systems. *Mathematical and Computer Modelling of Dynamical Sys-*

tems, **8**, 1–20.

[38] CHEN, S. AND BILLINGS, S. A. (1992). Neural networks for non- linear dynamic system modelling and identification. *International Journal of Control*, **56**, 319–346.

[39] PHA, D. T. (1995). *Neural Networks for Identification, Prediction and Control*. Springer.

[40] TESTUD, P., AUREGAN, Y., MOUSSOU, P. AND HIRSCHBERG, A. (2009). The whistling potentiality of an orifice in a confined flow using an energetic criterion. *J. Sound and Vibration*.

[41] KIERKEGAARD, A., ALLAM, S., EFRAIMSSON, M. AND ABOM, M. (2012). Simulation of whistling and the whistling potentiality of an in-duct orifice with linear aeroacoustics. *J. Sound and Vibration*.